COMBUSTION SCIENCE AND TECHNOLOGY
2017, VOL. 189, NO. 9, 1467–1485
https://doi.org/10.1080/00102202.2017.1305366

Taylor & Francis
Taylor & Francis Group

Numerical Investigation of the Stochastic Behavior of Light-Round in Annular Non-Premixed Combustors

Edouard Machover and Epaminondas Mastorakos

Department of Engineering, University of Cambridge, Cambridge, UK

ABSTRACT

The ignition behavior of a non-premixed multiple-burner annular combustion chamber was investigated numerically, focusing on the stochasticity and average speed of the light-round mechanism ensuring flame propagation from burner to burner that have been observed experimentally. During the propagation sequence, the flame expansion process is tracked by a previously developed stochastic low-order ignition model adapted to full combustor ignition. A stochastic model based on the probability that a flame fragment coming from an ignited burner leads to successful ignition of the next un-ignited one is developed in order to explain and quantify the global ignition behavior of the combustor. The stochastic behavior of the rig, highlighted through the experimentally observed variability of the burner-to-burner propagation times during the ignition sequence, was clarified and quantified. The lean light-round ignition limiting conditions and the mean light-round speed measured experimentally are explained and reasonably accurately predicted, demonstrating the validity of the use of the probabilistic model together with the low-order ignition model for the combustor considered. The results presented in this paper can be used to predict the ignition envelope of annular gas turbines combustors at the design stage.

ARTICLE HISTORY
Received 13 October 2016
Revised 8 February 2017
Accepted 8 March 2017

KEYWORDS
Flame propagation; Gas turbines; Ignition probability; Light-round; Non-premixed flames; Spark ignition

Introduction

Ignition of gas turbine combustors and rocket engines is important from a practical perspective and involves complex phenomena (Lefebvre, 1999; Mastorakos, 2009). The ignition process in gas turbines occurs in four phases Mastorakos (2009); Lefebvre (1999). The first phase is the generation of a kernel consisting of the initiation of a flame through a spark in a flammable mixture (Glassman and Yetter, 2008; Lefebvre, 1999; Lewis and von Elbe, 1987; Spalding, 1979). The second phase is flame propagation from the kernel. The third phase is the overall burner ignition characterized by the stabilization of the flame on a single injector. Stabilization is based on the physical mechanism of initiating combustion by bringing hot gases in contact with the reactants (Dunn-Rankin, 2008). The fourth phase is burner-to-burner flame propagation called light-round, which has not been yet extensively studied in the laboratory. This latter phase is the topic of this article, and in particular the probabilistic behavior of the underlying processes for annular non-premixed systems.

CONTACT Edouard Machover edouard.machover@gmail.com Department of Engineering, University of Cambridge, Trumpington Street, Cambridge CB2 1PZ, UK.

Color versions of one or more of the figures in the article can be found online at www.tandfonline.com/gcst.

In the context of single combustors, ignition has been studied experimentally (Lang et al., 2010; Mosbach et al., 2010; Read et al., 2010). Spark ignition has also been studied experimentally for non-premixed flames in various geometries (Ahmed et al., 2007a, 2007b; Ahmed and Mastorakos, 2006, 2010, 2016) and through Large Eddy Simulation (LES) (Bulat et al., 2013; Jones and Prasad, 2011; Jones et al., 2012; Lacaze et al., 2009; Subramanian et al., 2010; Triantafyllidis et al., 2009). Moreover, low-order ignition models providing lower computational cost have been developed in order to provide easier prediction of the ignition behavior in non-premixed and spray single burners (Eyssartier et al., 2013; Neophytou et al., 2012). In addition, the ignition behavior of single premixed burners have been investigated with the model developed by Neophytou et al. (2012) and Sitte et al. (2016).

For multiple burners, light-round has been studied in premixed configurations through experiments and simulations (Barré et al., 2014; Bourgouin et al., 2013; Machover, 2016; Machover and Mastorakos, 2017; Philip et al., 2015), following an initial numerical study of a helicopter engine Boileau et al. (2008).

Recently, in non-premixed configuration, light-round has been investigated experimentally and numerically by Machover and Mastorakos (2016) with a linear combustor comprising five non-premixed swirl bluff-body burners. Results have suggested that, in the inter-burner region, bridges of positive albeit small flammability factor—defined as the local probability of finding a mixture within the flammability limits [see Mastorakos (2009) for a review of this concept]—allow flame fragments to travel from the recirculation zone of the ignited burner to the recirculation zone of the adjacent one, leading to burner-to-burner propagation. Furthermore, fuel supply appeared to be of major importance to successful propagation. Indeed, very low values of flammability factor measured in the bridges allowed a flame fragment to travel from burner to burner only seldom.

Experimentally, burner-to-burner flame propagation has been further investigated by Machover and Mastorakos (2016) in an annular non-premixed combustion chamber adapted from the premixed combustor used by Worth and Dawson (2013a, 2013b) consisting of a variable number of equally spaced swirling burners equipped with a central bluff-body and axial fuel injection. The global light-round behavior of the annular combustor comprising N_b = 12, 15, or 18 burners was studied by investigating changes in spacing between burners (S), overall equivalence ratio (ϕ), and bulk velocity (U_b). Side visualization showed that burner-to-burner propagation occurring in the stratified inter-burner region consisted of a successful flame propagation event following a succession of failed events in which a flame fragment coming from the ignited burner failed to penetrate fully in the recirculation zone of the adjacent unignited burner. Turbulent dispersion process was considered dominant given that the time taken for successful burner-to-burner flame propagation was much larger than in premixed systems investigated in Bourgouin et al. (2013); Philip et al. (2015); Barré et al. (2014); Machover (2016); and Machover and Mastorakos (2017). The number of failed events appeared to vary significantly from burner to burner suggesting a stochastic global behavior. The variability was found to increase with augmenting S, diminishing ϕ, and increasing U_b. Furthermore, the average speed of light-round augmented with increasing number of burners or with increasing overall equivalence ratio. However, it remained rather constant with augmenting bulk velocity.

Following that experimental work, the present article aims to explain, through modelling, the above trends. First, the numerical set-up is presented. Then, a probabilistic model is developed in order to explain the stochastic behavior observed in the experiment. The experimental results obtained are then re-analyzed and explained with emphasis on the

stochasticity quantified through the model. Finally, the article concludes on the performance of the ignition and probabilistic models together for the prediction of ignition behavior in non-premixed configuration.

Methods

Burner description

The combustor modeled in the present work is represented by drawings and a photograph in Figure 1 and Figure 2, respectively, and is described in detail in Machover and Mastorakos (2016). This annular non-premixed combustion chamber consists of a variable number of equally spaced bluff-body stabilised turbulent non-premixed burners placed in an annular configuration. The air is exhausted through a plenum connected to 12, 15, or 18 identical 150 mm long circular tubes with an inner diameter of D = 18.9 mm. Each tube is fitted with a centrally located duct that consists in a 5-mm-diameter tube of wall thickness 1.0 mm. To the end of the duct, at the exit of the burner, a conical bluff-body of diameter D_a = 13 mm is attached, giving a blockage ratio of 50%. Each duct is connected to the methane supply. The pipe/bluff-body assemblies are arranged around a circle of diameter 170 mm and fixed between upper and lower plates. A six vane, α = 60°,

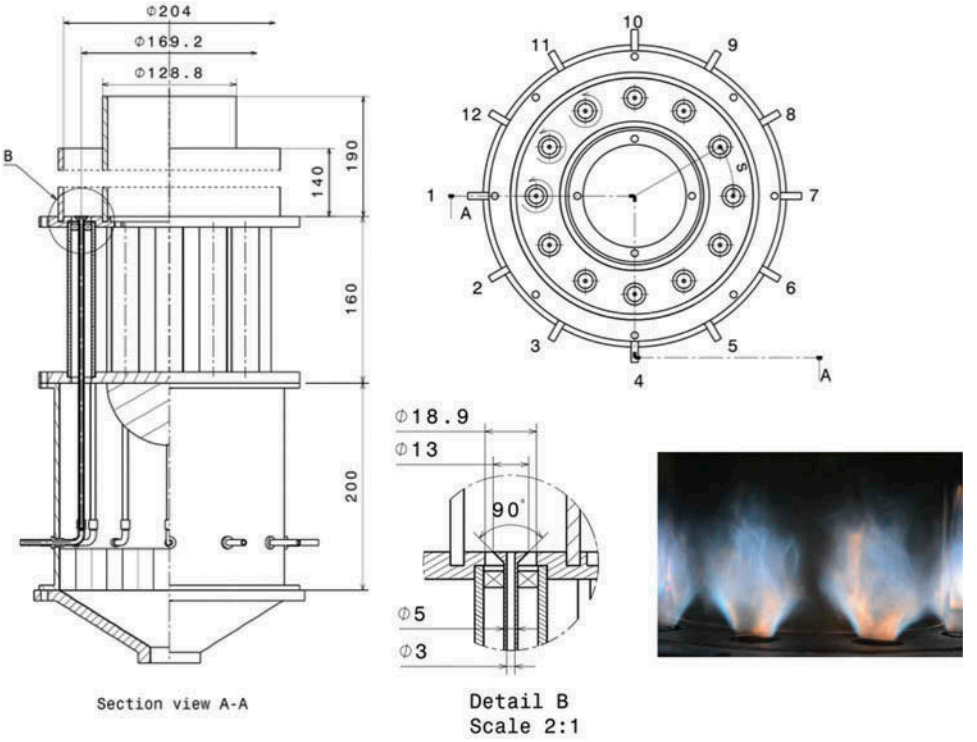

Figure 1. Drawing of the annular non-premixed combustor in the 12-burner configuration. Circular arrows indicate the direction of the swirl. The burners, separated by arc distance S, are numbered counter-clockwise. The dimensions are in mm. A photograph of flame 12_0.30_10 is shown. Dimensions are in mm.

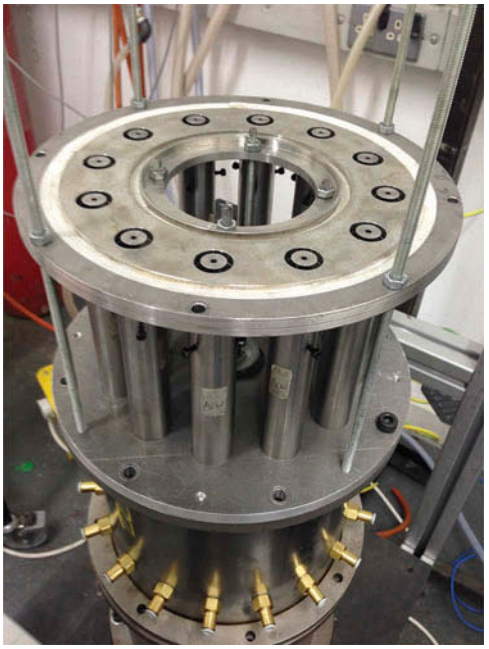

Figure 2. Overhead photograph of the assembly in the 12-burner configuration.

counter-clockwise swirler (as viewed from the top of the combustion chamber) is fitted 10 mm upstream of each of the bluff-body giving a geometrical swirl number of 1.22 Worth and Dawson (2013a). The flames are confined within an annular enclosure that consisted of inner and outer tubes of diameter D_{in}=127 mm and D_{out}= 212 mm. Three sets of plates were manufactured with the same circumference enabling simulations with 12-, 15-, and 18-burner configurations to be performed. These correspond to inter-burner spacings of $S_{12} = 2.33D$ ($S = 44.0$ mm), $S_{15} = 1.87D$ ($S = 35.3$ mm), and $S_{18} = 1.56D$ ($S = 29.5$ mm), where S denotes the arc distance between the bluff-body centers. In the study, flame characterized by inter-burner spacing S, overall equivalence ratio Φ, and bulk velocity U_b is denoted flame $S\_\phi\_U_b$.

Flow conditions

Flow conditions are the same as those studied experimentally in Machover and Mastorakos (2016). The process of light-round is investigated in ambient conditions of temperature ($T = 293$ K) and pressure (1 bar) with air/methane mixtures at three inter-burner spacings $S = S_{12}$, $S = S_{15}$, and $S = S_{18}$; at three overall equivalence ratios $\phi = 0.30$, $\phi = 0.35$, and $\phi = 0.40$; and at bulk velocities of air and methane reported in Table 1. Although these bulk velocities are lower than that encountered in realistic gas turbines, flow is turbulent in the combustion chamber (Reynolds numbers based on the bulk velocity at each burner's annular inlet and D range from $Re = 3950$ to $Re = 7100$). The flammability limits of the air-CH_4 mixture are $\xi_{lean} = 0.028$ and $\xi_{rich} = 0.089$; $\xi_{st} = 0.055$ is the stoichiometric mixture fraction (Turns, 2000).

Table 1. Flow conditions investigated numerically for the annular non-premixed burner.

Flame	Φ	U_{air} [m/s]	U_{CH_4} [m/s]
S_0.30_10	0.30	9.7	5.9
S_0.30_14	0.30	13.6	8.2
S_0.30_18	0.30	17.5	10.6
S_0.35_10	0.35	9.6	6.8
S_0.35_14	0.35	13.5	9.6
S_0.35_18	0.35	17.4	12.3
S_0.40_10	0.40	9.6	7.8
S_0.40_14	0.40	13.4	10.9
S_0.40_18	0.40	17.3	14.0

U_{air} and U_{CH_4} refer to the bulk velocity of the air at the end of the tubes and of the methane at the duct exit, respectively. Experimental conditions are tested for the three spacings $S = S_{12}$, $S = S_{15}$, and $S = S_{18}$.

Low-order modeling

The burner-to-burner propagation is investigated numerically by use of a low-order ignition model, i.e., based on a steady-state cold flow CFD solution without simulating transient flow, introduced first and fully described by Neophytou et al. (2012). Low-order models provide simplified and fast modeling of ignition compared to models with reacting flows. In the present model, flame propagation is modeled by the motion of virtual flame particles in a turbulent flow field, leaving the thermal environment apart. The required input for the code to simulate ignition events is a time-averaged cold flow solution.

The fluid domain is filled with rectangular grid cells of size Δx and the algorithm follows a cellular automaton model, i.e., the state of each cell changes over time according to some fixed rules. Cells can transit through two different states successively: cold state and burn state. The initial state is cold for all the cells. The spark is simulated by switching the cells in the spark volume from the cold to the burnt state. A burnt cell can not get back to its previous cold state. When a cell switches its state from cold to burnt, a single virtual flame particle is emitted. The dynamics of the flame particles is modeled by a simplified Langevin model described by the stochastic differential Equations (1) and (2) (Pope, 2000). Whenever a virtual flame particle enters a cold cell, the latter switches to the burnt state and emits one additional flame particle. In the present model, the ignition impact on the cold flow field is not considered and the mixture supply within the combustion chamber is not included.

$$\Delta X_{p,i} = U_{p,i}\Delta t \tag{1}$$

$$\Delta U_{p,i} = -\left(\tfrac{1}{2} + \tfrac{3}{4}C_0\right)\left(\tfrac{L_{turb}}{u'}\right)(U_{p,i} - \widetilde{U}_i)\Delta t + (C_0\varepsilon\Delta t)^{1/2}N_{p,i} \tag{2}$$

The latter equation consists in a linear drift towards the local time (isothermal) averaged velocity and an isotropic diffusion term. $\Delta X_{p,i}$ denotes the distance a particle p travels in the direction i during the time step Δt with velocity $U_{p,i}$. C_0 is a constant equal to 2.0 and N_p a random variable that follows a normal distribution of mean 0 and standard deviation 1. The cold flow time-averaged CFD solution provides the other parameters. u' denotes the turbulent velocity fluctuation estimated as $\sqrt{k}$, where k is the turbulent kinetic energy, L_{turb} the integral length scale, $\widetilde{U}_i$ the local mean velocity, and ε the local turbulent dissipation rate.

Moreover, an extinction criterion based on the local Karlovitz number (Ka) and originally introduced by Abdel-Gayed and Bradley (1985) is applied to decide whether a

flame particle remains active or not. The flame particle quenches if Ka_p exceeds the critical value $Ka_{crit} = 1.5$ (Abdel-Gayed and Bradley, 1985). The local Karlovitz number is calculated for each flame particle at every time step according to Equation (3).

$$Ka_p = 0.157\left(\nu\frac{(u')^3}{L_{turb}}\right)^{1/2}\frac{1}{S_L^2} \tag{3}$$

Here ν is the kinematic viscosity and S_L the laminar flame speed. S_L depends on the local mean mixture fraction ξ and is calculated by the ignition model according to data provided by Vagelopoulos and Egolfopoulos (1998) for methane. ξ, L_{turb}, and u' are provided everywhere within the combustion chamber by the cold flow CFD solutions used as an input for the low-order model. Locally, the mixture fraction follows a β-function probability density function (PDF) with mean and root mean square (r.m.s.) given by the cold flow CFD solution. The flammability factor F is calculated assuming a β-function PDF for the mixture fraction. The local mixing is taken into account as the local Ka diverges when the local mixture is not flammable (S_L is zero), resulting in virtual flame particle quenching given that the limit set by the extinction criterion is exceeded.

The model, as described above, has been validated for ignition of non-premixed and spray recirculating flames (Neophytou et al., 2012), bluff-body premixed flames (Sitte et al., 2016), and realistic gas turbine combustors (Neophytou et al., 2011; Soworka et al., 2013), and is illustrated in Figure 3, where virtual particle quenching following two burning particle emissions is sketched.

Criteria based on some quantities relative to the cold flow have been proposed by Neophytou et al. (2012) for the choice of the time step (Δt) and the grid size (Δx). First, the time-step Δt should be smaller than the large-eddy time-scale for all the turbulent time scales to be captured by the code. The time-step being fixed, grid spacing boundaries are determined from the Langevin model. $\forall p, i$, $\Delta X_{p,i}$ should be smaller than the distance a particle is carried by an eddy during Δt. Finally, the grid spacing should be larger than the smaller turbulent scales. In the turbulence spectrum, the middle of the dissipation range in

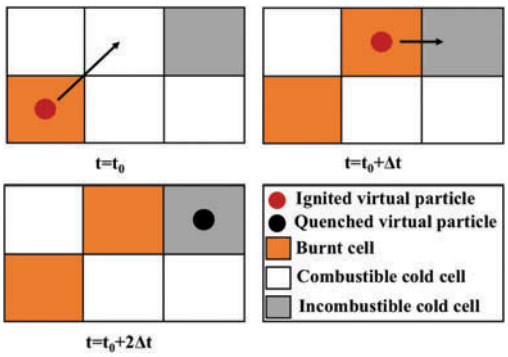

Figure 3. Illustration of a single flame fragment propagation with the low-order model. In this example, a virtual burning particle is emitted from an ignited cell at $t = t_0$. Following the trajectory given by the simplified Langevin model (represented by the arrow in the figure), it reaches a combustible cold cell at $t = t_0 + \Delta t$ that switches its state from cold to burnt. Then, the burnt state emits a virtual burning particle that attains an incombustible cold cell at $t = t_0 + 2\Delta t$, resulting in virtual particle extinction.

the Kolmogorov scale is at approximately $18\eta_K$, where η_K is the Kolmogorov length scale (Pope, 2000). Regarding those guidelines, the retained values are $\Delta x = 2.0$ mm and $\Delta t = 0.5$ ms.

Cold flow CFD solution

Time-averaged CFD cold flow solutions of the 27 different flames described in Table 1 were computed with LES with the commercial software ANSYS Fluent. The incompressible Navier–Stokes equation solutions were obtained with the Smagorinsky–Lilly subgrid-scale model with default model constants. Spatial discretization was set up with least square cell based gradient reconstruction, second order upwind momentum, and second order mean mixture fraction. Finally, a bounded second order implicit transient formulation was adopted together with the PISO scheme for the pressure-velocity coupling. The computational domain comprised one single burner sector of the rig consisting of 1/12, 1/15, or 1/18 of the annular combustor. The domain was meshed with an unstructured tetrahedral grid refined in the region of the recirculation zone, and in the air and the fuel inlets. The grid for the 12-, 15-, and 18-burner configuration comprised 7.7×10^5, 7.3×10^5, and 6.5×10^5 cells corresponding to 1.5×10^5, 1.4×10^5, and 1.3×10^5 nodes, respectively, with minimum size 0.5 mm and maximum size 1.8 mm. At the exit of the air inlet, the tangential component of the flow induced by the swirl was set equal to the axial component following the velocity field experiments conducted in a non-premixed linear combustion chamber presenting very similar flow characteristics (Machover, 2016). This single unit had periodic boundary conditions on the walls disposed at the middle of the arc distance between burners. For the use of the cold flow field as an input in the low-order model, each individual burner CFD solution was interpolated on a regular grid of 2.0 mm spacing. For each case, the CPU time required by the desktop machine used (8 CPUs, Intel(R) Core(TM) i7-4820K @3.70Ghz, 32 GB RAM) was approximately 40 h. The full combustor CFD solution was obtained by concatenating the 12, 15, or 18 interpolated units. The CPU time required to compute 500 ignition trials with the low-order ignition model SPINTHIR (Stochastic Particle INTegrator for High-altitude Relight) was about 5 h with the desktop PC.

Stochastic light-round modeling

It has been shown experimentally that burner-to-burner propagation occurring in the inter-burner region consisted of a successful flame propagation event following a succession of failed events in which a flame fragment coming from the ignited burner failed to penetrate fully in the recirculation zone of the adjacent un-ignited burner (Machover and Mastorakos, 2016). The main idea of the following probabilistic model is to model the burner-to-burner propagation by a succession of failed and successful events occurring with a certain probability. A successful event corresponds to a flame fragment emitted from an ignited burner that successfully ignites the next un-ignited one.

We denote by δt the average time a flame fragment would take to travel from any ignited burner to any un-ignited adjacent one. We now denote by P the probability that during δt, the flame fragment leads to successful ignition of the burner. P depends on various parameters such as S, ϕ, U_b, and the inter-burner turbulent pattern that is time dependant. If $\delta t > T_{turb} = L_{turb}/U_b$, T_{turb} being the large-eddy turnover time, a flame

Table 2. The ratio $\delta t/T_{turb}$ for the various conditions simulated, which assists in assessing the applicability of the probabilistic model.

Φ	$U_b = 10$ m/s	$U_b = 14$ m/s	$U_b = 18$ m/s
12-burner configuration			
0.30	4.1	2.1	∞
0.35	3.9	3.5	3.3
0.40	2.9	2.1	2.0
15-burner configuration			
0.30	3.2	1.5	∞
0.35	3.0	1.9	1.3
0.40	2.6	1.8	1.3
18-burner configuration			
0.30	2.5	1.1	∞
0.35	1.9	1.0	1.1
0.40	1.7	1.2	0.8

δt is calculated with the low order-ignition model. T_{turb} is obtained numerically with the LES cold flow solution.

fragment experiences all the turbulent time scales during δt. Thus, all the flame fragments experience the same turbulent environment in the inter-burner region and P is reduced to a function of S, ϕ, U_b only, assuring that the sequence of events is independent and identically distributed. This hypothesis is verified *a posteriori* (Table 2).

Suppose an ignited burner (index $k-1$) and let us determine the average time taken to ignite the adjacent un-ignited one (index k). The probability $P_{\delta t}$ that successful burner-to-burner propagation occurs during δt is given by:

$$P_{\delta t} = P \tag{4}$$

Burner-to-burner propagation is successful in $k\delta t$ if a successful event follows $k-1$ unsuccessful ones. The probability associated, $P_{k\delta t}$ is hence given by:

$$P_{k\delta t} = (1-P)^{k-1}P \tag{5}$$

The average propagation time that takes a flame fragment to travel from one burner to the adjacent one *i.e.* the expected value of the burner-to-burner propagation time, $\bar{T}$, is given by:

$$\bar{T} = \sum_{i=1}^{\infty} P_{k\delta t} k\delta t = P\delta t \sum_{i=0}^{\infty} k(1-P)^k \tag{6}$$

Thus, the problem is reduced to a geometric sequence with success probability P. The expected value of a geometrically distributed random variable being $\frac{1}{P}$, the average propagation time from burner to burner is given by:

$$\bar{T} = \frac{\delta t}{P} \tag{7}$$

Finally, considering that the average speed of light-round S_{LR} is given by:

$$S_{LR} = \frac{S}{\bar{T}} \tag{8}$$

where S is the arc distance between two burners and that the average speed at which flame propagates during an event, V_{LR}, is given by:

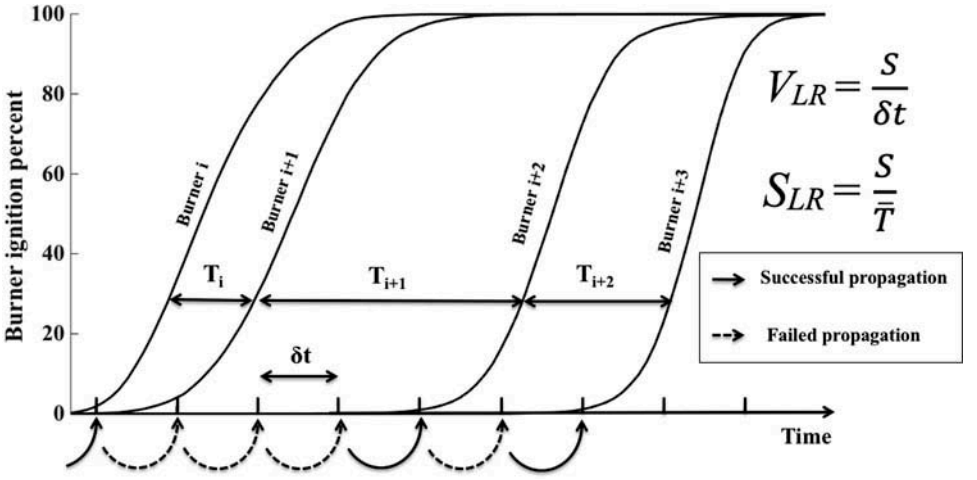

Figure 4. Illustration of the burner-to-burner propagation model. In this example, the first burner has already been ignited. A successful event results in the ignition of the second one. Then, the succession of three failed events followed by a successful event leads to the ignition of the next burner. The last burner ignites after a failed followed by a successful event.

$$V_{LR} = \frac{S}{\delta t} \tag{9}$$

we obtain the final relation:

$$S_{LR} = P.V_{LR} \tag{10}$$

The model is illustrated in Figure 4, where a succession of four consecutive burners ignition is sketched.

P and V_{LR} are determined with the low order ignition model by performing simulations of a large number of full combustor ignition events, N_e, presently 500. The study focuses strictly on the burner-to-burner propagation mechanism. Thus, it is assumed that the first burner of the annular combustion chamber was always successfully ignited. Consequently, results presented herein do not take into account ignition of the first burner. For each ignition sequence, burner-to-burner propagation is initiated by a 10 mm diameter spark situated in the first burner, leading to its successful ignition. The probability P that flame travels successfully from one burner to the next one can be quantified since the code does not take into account refuelling. Indeed, since virtual particles that had extinguished cannot go back to their previous ignited state, one failed event results in the cessation of burner-to-burner propagation. In other terms, the bridges of positive flammability factor can be used only once by the flame fragment. Therefore, the first burner being always successfully ignited, the i-th burner in succession to the sparked one ($i \in [1, N_b - 1]$) will have a probability P^i to be ignited long-term, in steady-state. Hence, after having performed N_e simulations, the number of successful ignition N_i of a burner i leads to the determination of $P = (N_i/N_e)^{1/i}$. This probability does not take into account the probability to ignite the first burner. Furthermore, V_{LR} is obtained by dividing the distance $i.S$ by the average time taken by the flame to travel from the first burner to the i-th burner. In practice, i was chosen as close as possible to the burner number opposite to the first one with values of P^i greater than zero.

Results and discussion

In this section, burner-to-burner flame propagation is investigated numerically with the low-order ignition model together with the probabilistic model in order to quantify the stochasticity of the process. The stochastic behavior of the combustor, the lean light-round ignition limits and the mean light-round speed measured experimentally are examined.

Cold flow and flame propagation pattern

Cold flow CFD solutions obtained with LES are shown for flame 12_0.40_18 in Figure 5. The axial component of the velocity takes high values in the expanding annular flow coming out from the burner air inlet and in the central gas jet. A central recirculation zone is observed. Small side recirculation zones are also visible at the limit of the annular jet formed by the expanding flow. The flammability factor takes high values in the expanding annular air inlet region, small values in the central jet region, and bridges of small flammability factor in the inter-burner region are visible. Generally, the flow is very similar to that from a non-premixed configuration studied in detail by Machover and Mastorakos (2016), where a full flow description is provided.

Burner-to-burner propagation modeling is shown in Figure 5, where flame spread around the annular combustor is tracked with the low-order ignition model in the 12-burner configuration for flame 12_0.40_18. One failed propagation from burner to burner (from the central burner to that on the left) and one successful burner-to-burner flame

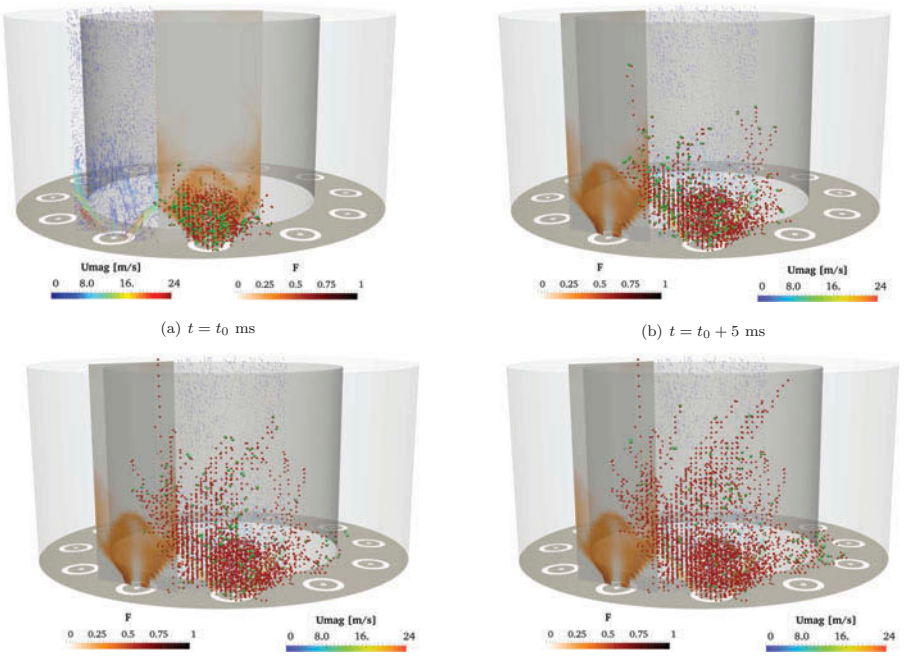

(a) $t = t_0$ ms (b) $t = t_0 + 5$ ms

(c) $t = t_0 + 10$ ms (d) $t = t_0 + 15$ ms

Figure 5. Side view of a successful and failed burner-to-burner flame propagation obtained with the low-order model for flame 12_0.40_18. The annular non-premixed burner is sketched. Burning and extinguished flame virtual particles are represented in green and red, respectively.

propagation (from the center burner to that on the right) are shown. In both cases, burning virtual particles spread into the region of the sparked burner ($t = t_0$ ms) and are convected downstream into the adjacent burner region ($t = t_0 + 5$ ms). Either all burning particles extinguish along the bridge of small flammability factor in the inter-burner region ($t = t_0 + 15$ ms) and burner-to-burner propagation does not occur (failed propagation from the central burner to the left adjacent one), or burning virtual particles successfully reach the recirculation zone of the adjacent un-ignited burner (successful propagation from the central burner to the left one). These numerical results are in accordance with that experimentally observed in Machover and Mastorakos (2016), where a failed and a successful propagation sequence are shown.

Ignitability limits

For all the flames studied, the calculated probability of successful propagation is plotted as a function of the bulk velocity and overall equivalence ratio for different inter-burner spacings in Figure 6, together with the lean light-round propagation limit obtained experimentally by Machover and Mastorakos (2016) in Figure 7. The lean light-round propagation limit circumscribes the stable lightround region where successful propagation occurs in the long term and the region where the burner-to-burner propagation never occurs. Beyond the lean light-round ignition limit, any (U_b,ϕ) point at fixed S leads to successful burner-to-burner propagation, whereas below that limit, no light-round occurs. The probabilities P of successful light-round, as given by the model, are denoted by the color of the square in Figure 7. A few trends are clearly visible. First, decrease of the inter-burner spacing results generally in increase of P. Indeed, a decrease of the length of the bridges of small flammability factor between the burners results in a greater probability for a flame fragment not to extinguish during its propagation. Second, an increase in overall equivalence ratio leads to an increase of P, resulting from the higher values of flammability factor in the inter-burner area evidenced in Machover (2016) where detailed laser diagnostics have been performed in a linear non-premixed combustion chamber adapted from that of the present study. Third, a bulk velocity increase mostly results in a decrease of P, a

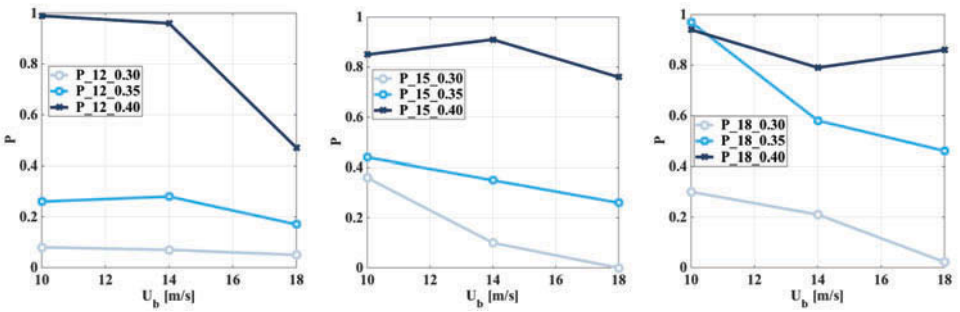

(a) $S = S_{12}$ (b) $S = S_{15}$ (c) $S = S_{18}$

Figure 6. Simulated probability of successful propagation as a function of the bulk velocity and different overall equivalence ratios for the flames studied. Each image shows a different inter-burner spacing: (a) 12 burners, (b) 15 burners, and (c) 18 burners.

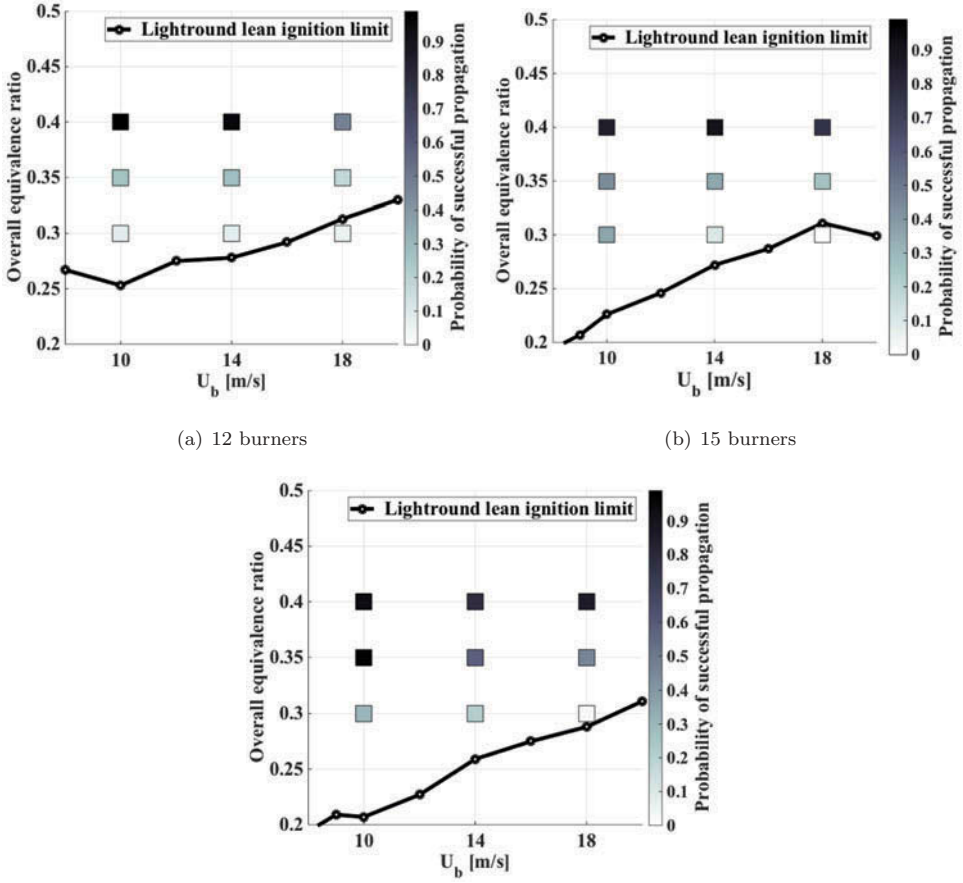

(a) 12 burners

(b) 15 burners

(c) 18 burners

Figure 7. Simulated P and lean light-round ignition limits measured experimentally in Machover and Mastorakos (2016) in the (U_b,ϕ) space for three inter-burner spacings: (a) 12-burner, (b) 15-burner, and (c) 18-burner configurations. The color of each square represents the probability obtained by the simulation.

trend explained by flame fragments more inclined to quench in an environment with higher strain rate. In general, the model provides a diminishing P as the experimentally observed lean ignition limit is approached, which suggests that the model has promising predictive capability.

These results explain the light-round envelopes obtained experimentally. At fixed U_b, with gradually diminishing ϕ, P decreases until it reaches zero preventing propagation from burner to burner. The result is illustrated for flames out of the stable light-round region or close to its limit at small overall equivalence ratio and high bulk velocity (S_0.30_18), as P drops to zero for the three inter-burner spacings considered, explaining that in these conditions, no burner-to-burner propagation was observed experimentally (Machover and Mastorakos, 2016). Furthermore, for every inter-burner spacing configuration, at fixed ϕ, P decreases with an increase in U_b. This explains the positive slope of the lean light-round ignition limits evidenced experimentally given

that with bulk velocity increase, higher overall equivalence ratio is necessary for successful burner-to-burner propagation. Finally, for every inter-burner spacing configuration, at fixed ϕ and U_b, increase in P with an inter-burner spacing decrease explains the wider ignition envelopes obtained experimentally in Machover and Mastorakos (2016). Future work could consist in full ignition envelopes prediction by simulating $S\_0.20\_U_b$ and $S\_0.25\_U_b$ flames.

Variability

The measurements conducted on the annular non-premixed combustor showed that the time taken between two consecutive burner ignitions varied significantly during the burner-to-burner propagation sequence (Machover and Mastorakos, 2016). This variability was found to be higher by decreasing the number of burners, by diminishing the overall equivalence ratio and by increasing the bulk velocity (Machover and Mastorakos, 2016). The probability density function (PDF) of the experimentally measured propagation time between two consecutive burners and the PDF of the geometric distribution at each value in time using the simulated probability P represented in Figure 6 are plotted together in Figure 8 for four different flames. The geometric distribution fits reasonably well with the experimental values. This shows that the burner-to-burner propagation time follows actually a geometric distribution of success probability P that is very close to the simulated one. Moreover, the variability trends observed are explained by the probabilistic model. Indeed, it is shown in Figure 8 that the variability increases with an increase in U_b at fixed S and ϕ (Figures 8a and 8b), with a decrease in ϕ at fixed S and U_b (Figures 8a and 8c) and with a reduction of number of burners at fixed ϕ and U_b (Figures 8b and 8d), all of which is explained by the drop of P highlighted above.

Time of complete ignition and flame speed

The effects of variations in U_b, in ϕ, and in S on the average speed of successful propagation of a flame fragment V_{LR} are shown in Figure 9. Again, some trends are clearly visible. First, at fixed ϕ and U_b, a decrease in the inter-burner spacing results in a higher V_{LR}. This can be explained by the lower path a flame fragment would travel in the bridges that follow the radially expanding annular air inlet, as shown in Machover (2016). Second, at fixed S and ϕ, increasing U_b mostly results in the increase of V_{LR}, a trend explained by the faster convection by the flow. Third, when increasing ϕ, with S and U_b remaining fixed, there is tendency for higher speed of successful propagation, although a strong correlation was not obtained.

Experimentally, for every configuration, the average speed of light-round S_{LR} (defined by the average speed at which burner-to-burner propagation occurs) was determined by averaging a number of individual burner-to-burner propagation speeds Machover and Mastorakos (2016). These results are compared with the values of $S_{LR} = P.V_{LR}$, with P and V_{LR} obtained numerically with the low order ignition model, at fixed inter-burner spacing in Figure 10.

The results obtained showed that $\delta t > T_{turb}$ except for flame 18_0.40_18 as shown in Table 2. Consequently, the model is valid in regard to the applicability hypothesis for all the other flames.

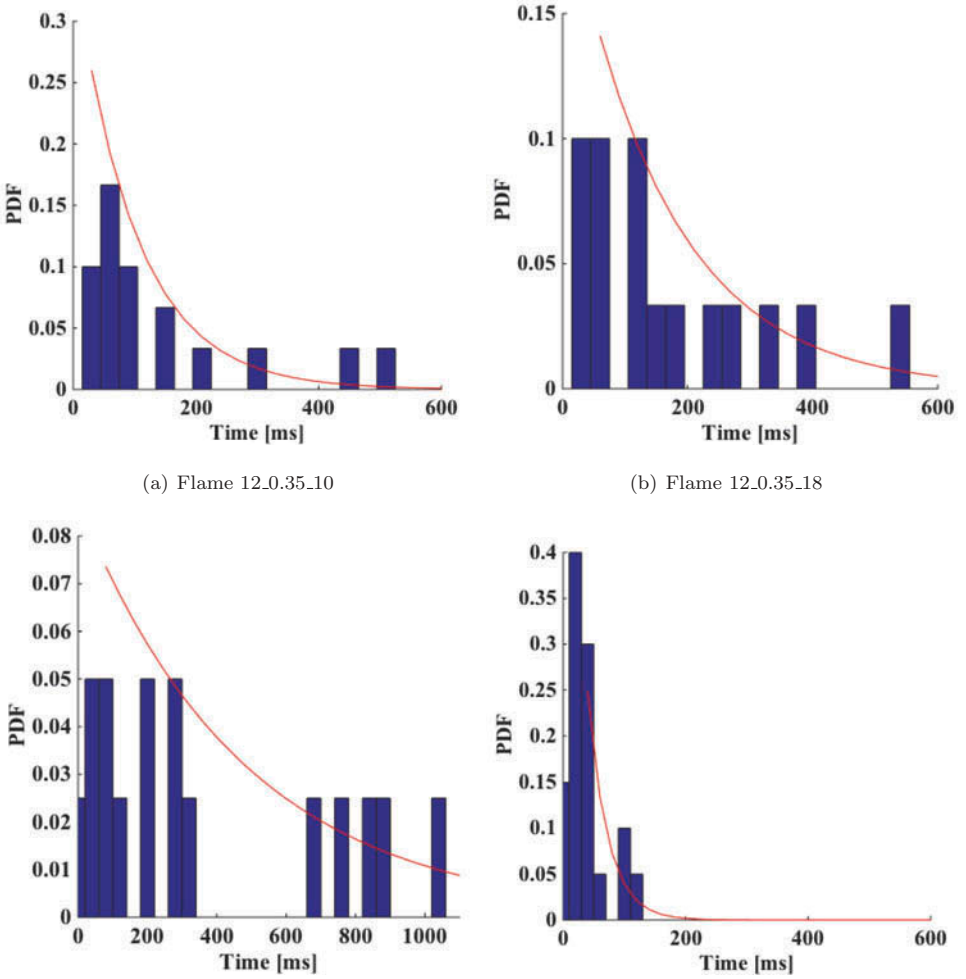

(a) Flame 12_0.35_10

(b) Flame 12_0.35_18

(c) Flame 12_0.30_10

(d) Flame 18_0.35_18

Figure 8. PDF of the time between consecutive burner ignitions determined experimentally. The red curve represents the geometric distribution PDF associated to the simulated P. The effects of increase in bulk velocity, (a) and (b), decrease in overall equivalence ratio, (a) and (c), and decrease in inter-burner spacing, (b) and (d), are shown.

At high inter-burner spacing and low overall equivalence ratio, the experimental data are correctly retrieved with accurate prediction of a number of trends and values by the numerical model. Indeed, as shown in Table 2, δt approaches T_{turb} for high overall equivalence ratio and small inter-burner spacing, which can explain the better applicability of the model for very lean mixtures and high inter-burner spacing, as shown in Figure 10. These results show both some ability of the code to track the propagation of a flame from burner to burner, and the accuracy of the flame fragment propagation characterization that is the founding principle of the present probabilistic model. Furthermore, the experimental trends can be interpreted by the above expression of S_{LR}. Indeed, when fixing ϕ and U_b, a decrease of S results in the increase of P and V_{LR}

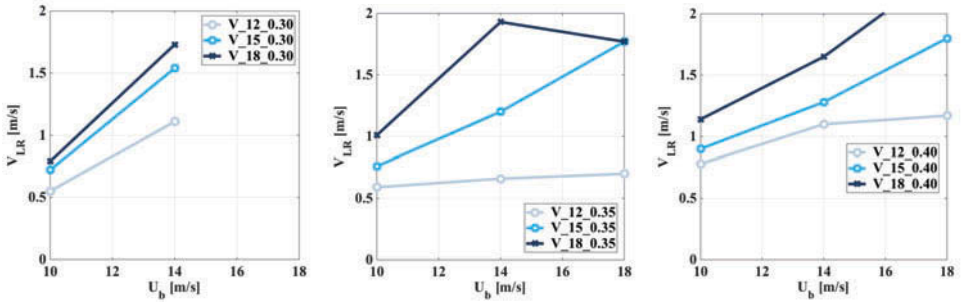

(a) $\phi = 0.30$ (b) $\phi = 0.35$ (c) $\phi = 0.40$

Figure 9. Simulated average speed of successful propagation V_{LR} as a function of the bulk velocity and different burner spacings for the flames studied. Each image shows a different overall equivalence ratio: (a) 0.30, (b) 0.35, and (c) 0.40. No simulated average speed of successful propagation could be determined for flames *S*_0.3_18 (*P* drops to zero).

together, explaining the increase of S_{LR} when increasing number of burners. Likewise, when fixing S and U_b, an increase of ϕ results in the increase of P and V_{LR} together, explaining the increase of S_{LR} when increasing the overall equivalence ratio. However, at fixed ϕ and S, an increase in U_b leads to decrease of P and increase of V_{LR} at the same time, a result interpreting the unexplained rather constant evolution of speed of light-round when increasing the bulk velocity evidenced in Machover and Mastorakos (2016). Finally, S_{LR} is proportional to the probability that a flame fragment travels successfully from burner to burner, which justifies the low light-round speeds found in these very lean stratified flows.

Conclusions

The ignition behavior of an annular non-premixed combustion chamber comprising 12, 15, or 18 individual bluff-body swirl non-premixed burners has been examined numerically focusing on the process of light-round, namely the burner-to-burner flame propagation. Previous experiments conducted with the same non-premixed combustion chamber have shown that the flame propagation has a stochastic nature; the probability that a flame fragment travels from one burner to the next controls the burner-to-burner propagation. A model based on the probability of a flame fragment to travel from one burner to the next has been developed in order to quantify the light-round process. Together with a stochastic low-order ignition model adapted to the present configuration, interpretations of experimental results obtained previously with the same combustor were made. First, the numerical results were in accordance with the lean burner-to-burner ignition limit general shape and the wider ignition envelopes obtained experimentally when diminishing the inter-burner spacing. Second, an approach of the stochastic global behavior was suggested by the statistical trends obtained with the probabilistic model. Thereby, the variability trends of the time taken from a burner to ignite the next one during the ignition sequence were interpreted by the numerical model. Finally, average speeds of light-round obtained numerically were in rather good agreement with those measured experimentally, especially at low overall equivalence ratio and large inter-burner spacing. Limitations of the model could explain some

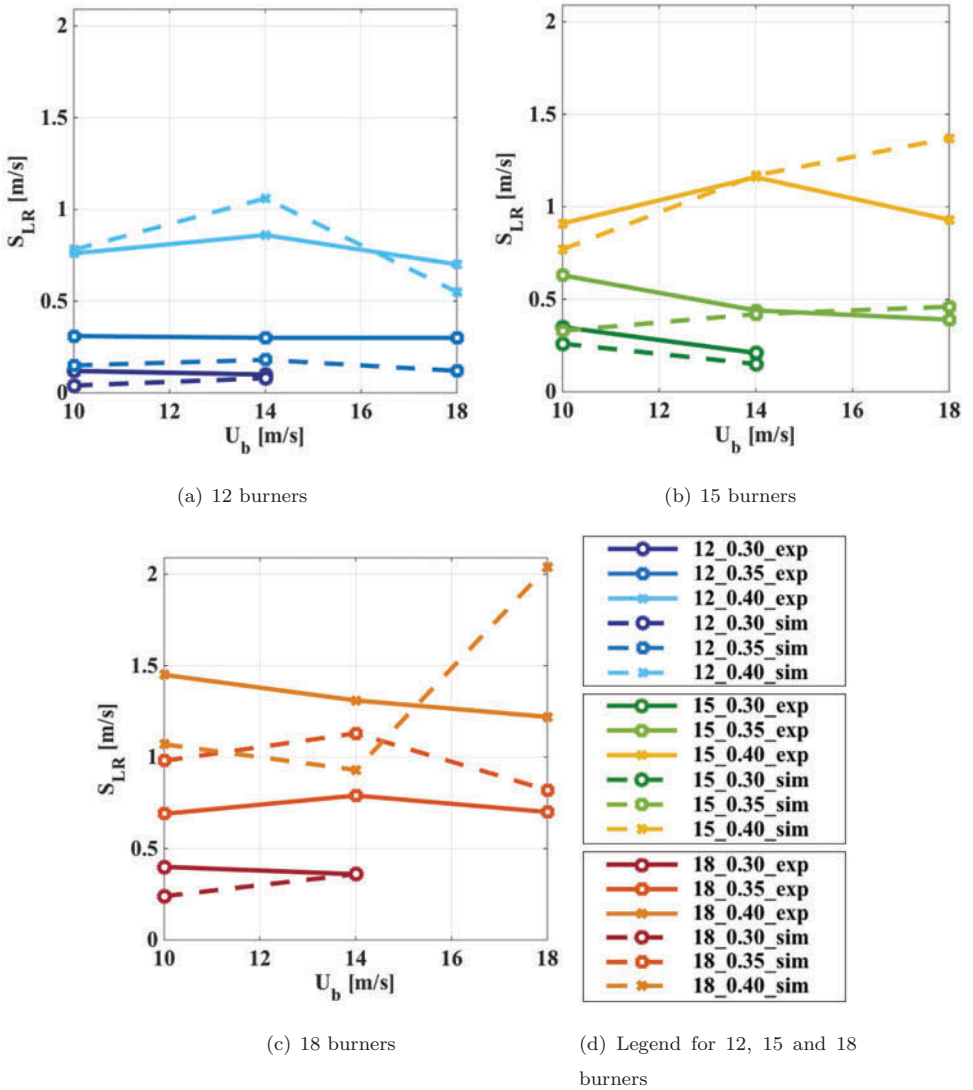

(a) 12 burners (b) 15 burners

(c) 18 burners (d) Legend for 12, 15 and 18 burners

Figure 10. Comparison of the experimental and simulated speeds of light-round as a function of the bulk velocity and different overall equivalence ratios, fixing the number of burners at (a) 12, (b) 15, and (c) 18. No simulated speeds of light-round could be determined for flames $S\_0.3\_18$ (P drops to zero). The experimental data come from Machover and Mastorakos (2016).

discrepancies between simulations and experiments at low spacing between burners and high overall equivalence ratios. The model allowed interpretation of the trends obtained when bulk velocity, overall equivalence ratio, and inter-burner spacing varied. The present work highlights the statistical nature of ignition in non-premixed annular systems.

In the present study, the lightround process has been investigated in inhomogeneous fuel/air mixtures. However, real gas turbines involve turbulent spray combustion and additional complexity arise with flame propagating across a droplet-laden air flow. Indeed, a series of interdependent physical phenomena occurs in two-phase flows: atomization

and evaporation of the liquid fuel, interaction between liquid droplets, turbulence and mixing in the gas phase, and process of forced ignition itself. Moreover, the present work has been conducted with laboratory-scale multiple-burner combustion chambers open downstream to the atmosphere at ambient conditions. In practice, relight occurs at high altitude and more research is necessary in order to study burner-to-burner flame propagation at different conditions of temperature and pressure. The present low-order model has shown good predictive capability of ignition probability trends in single burners operating with sprays (Neophytou et al., 2012). Moreover, effects of pressure and temperature variation are indirectly taken into account by the model through the laminar flame speed and the flammability factor contours.

Similar efforts in more complex configurations with liquid fuel spray flames at realistic conditions of temperature and pressure should be conducted in order to fully understand ignition in gas turbine annular combustors.

Nomenclature

N_b	number of individual burners of the annular combustor
D	inner diameter of the individual burners
δt	flame fragment average propagation time
P	flame fragment successful propagation probability
φ	overall equivalence ratio
S	inter-burner spacing
S_{LR}	average speed of light-round
T	average burner-to-burner propagation time
U_b	bulk velocity
V_{LR}	average speed of a flame fragment

Acknowledgment

We thank Mr. Philip Sitte for useful discussions on ignition modeling.

Funding

The authors acknowledge financial assistance from EPSRC though a Doctoral Training Award and Rolls-Royce Group.

ORCID

Epaminondas Mastorakos http://orcid.org/0000-0001-8245-5188

References

Abdel-Gayed, R., and Bradley, D. 1985. Criteria for turbulent propagation limits of premixed flames. *Combust. Flame*, **62**, 61–68.

Ahmed, S., Balachandran, R., Marchione, T., and Mastorakos, E. 2007a. Spark ignition of turbulent nonpremixed bluff-body flames. *Combust. Flame*, **151**, 366–385.

Ahmed, S., Balachandran, R., and Mastorakos, E. 2007b. Measurements of ignition probability in turbulent nonpremixed counterflow flames. *Proc. Combust. Inst.*, **31**, 1507–1513.

Ahmed, S., and Mastorakos, E. 2006. Spark ignition of lifted turbulent jet flames. *Combust. Flame*, **146**, 215–231.

Ahmed, S., and Mastorakos, E. 2010. Correlation of spark ignition with the local instantaneous mixture fraction in a turbulent nonpremixed methane jet. *Combust. Sci. Technol.*, **182**, 1360–1368.

Ahmed, S., and Mastorakos, E. 2016. Spark ignition of a turbulent shear-less fuel-air mixing layer. *Fuel*, **164**, 297–304.

Barré, D., Escalpez, L., Cordier, M., Riber, E., Cuenot, B., Staffelbach, G., Renou, B., Vandel, A., Gicquel, L., and Cabot, G. 2014. Flame propagation in aeronautical swirled multi-burners: Experimental and numerical investigation. *Combust. Flame*, **161**, 2387–2405.

Boileau, M., Staffelbach, G., Cuenot, B., Poinsot, T., and Berat, C. 2008. LES of an ignition sequence in a gas turbine engine. *Combust. Flame*, **154**, 2–22.

Bourgouin, J.F., Durox, D., Schuller, T., Beaunier, J., and Candel, S. 2013. Ignition dynamics of an annular combustor equipped with multiple swirling injectors. *Combust. Flame*, **160**, 1398–1413.

Bulat, G., Jones, W., and Marquis, A. 2013. Large eddy simulation of an industrial gas-turbine combustion chamber using the sub-grid pdf method. *Proc. Combust. Inst.*, **34**, 3155–3164.

Dunn-Rankin, D. 2008. *Lean Combustion: Technology and Control*, Academic Press, Burlington, MA.

Eyssartier, A., Cuenot, B., Gicquel, L., and Poinsot, T. 2013. Using LES to predict ignition sequences and ignition probability of turbulent two-phase flames. *Combust. Flame*, **160**, 1191–1207.

Glassman, I., and Yetter, R. 2008. *Combustion*, 4th ed. Academic Press, Burlington, MA.

Jones, W., Marquis, A., and Prasad, V. 2012. LES of a turbulent premixed swirl burner using the Eulerian stochastic field method. *Combust. Flame*, **159**, 3079–3095.

Jones, W., and Prasad, V. 2011. LES-pdf simulation of a spark ignited turbulent methane jet. *Proc. Combust. Inst.*, **33**, 1355–1363.

Lacaze, G., Richardson, E., and Poinsot, T. 2009. Large eddy simulation of spark ignition in a turbulent methane jet. *Combust. Flame*, **156**, 1993–2009.

Lang, A., Lecourt, R., and Giuliani, F. 2010. Statistical evaluation of ignition phenomena in turbojet engines. Presented at the ASME Turbo Expo 2010, Glasgow, UK, June 14–18; GT2010-23229, ASME, New York, 985–992.

Lefebvre, A. 1999. *Gas Turbine Combustion*, 2nd ed. Taylor and Francis, London.

Lewis, B., and von Elbe, G. 1987. *Combustion, Flames and Explosions of Gases*, Harcourt Brace Jovanovich, London.

Machover, E. 2016. Spark ignition in annular combustors. Ph.D. thesis, University of Cambridge.

Machover, E., and Mastorakos, E. 2016. Spark ignition of annular non-premixed combustors. *Exp. Therm. Fluid Sci.*, **73**, 64–70.

Machover, E., and Mastorakos, E. 2017. Experimental investigation on spark ignition of annular premixed combustors. *Combust. Flame*, **178**, 148–157.

Mastorakos, E. 2009. Ignition of turbulent non-premixed flames. *Prog. Energy Combust. Sci.*, **35**, 57–97.

Mosbach, T., Sadanandan, R., Meier, W., and Eggels, R. 2010. Experimental analysis of altitude relight under realistic conditions using laser and high-speed video techniques. Presented at the ASME Turbo Expo 2010, Glasgow, UK, June 14–18; GT2010-22625, ASME, New York, pp. 523–532.

Neophytou, A., Mastorakos, E., Richardson, E., Stow, S., and Zedda, M. 2011. A practical model for the high-altitude relight of a gas turbine combustor. Presented at the 7th Mediterranean Combustion Symposium, Chia Laguna, Cagliari, Sardina, Italy.

Neophytou, A., Richardson, E., and Mastorakos, E. 2012. Spark ignition of turbulent recirculating non-premixed gas and spray flames: A model for predicting ignition probability. *Combust. Flame*, **159**, 1503–1522.

Philip, M., Boileau, M., Vicquelin, R., Riber, E., Schmitt, T., Cuenot, B., Durox, D., and Candel, S. 2015. Large eddy simulations of an annular multiple-injector combustor. *Proc. Combust. Inst.*, **35**, 3159–3166.

Pope, S. 2000. *Turbulent Flows*, Cambridge University Press, London.

Read, R.W., Rogerson, J.W., and Hochgreb, S. 2010. Flame imaging of gas-turbine relight. *AIAA J.*, **48**, 1916–1927.

Sitte, M., Bach, E., Kariuki, J., Bauer, H.J., and Mastorakos, E. 2016. Simulations and experiments on the ignition probability in turbulent premixed bluff-body flames. *Combust. Theor. Modell.*, **20**, 548–565.

Soworka, T., Gerendas, M., and Eggels, R. 2013. Numerical investigation on ignition performance of a lean burn combustor at sub-atmospheric conditions. Proceedings of the ASME Turbo Expo 2013, Duusseldorf, Germany, June 16–20; GT2014–25644, ASME, New York.

Spalding, D. 1979. *Combustion and Mass Transfer*, Pergamon Press.

Subramanian, V., Domingo, P., and Vervisch, L. 2010. Large eddy simulation of forced ignition of an annular bluff-body burner. *Combust. Flame*, **157**, 579–601.

Triantafyllidis, A., Mastorakos, E., and Eggels, R. 2009. Large eddy simulation of forced ignition of a non-premixed bluff-body methane flame with conditional moment closure. *Combust. Flame*, **156**, 2328–2345.

Turns, S. 2000. *An Introduction to Combustion: Concepts and Applications*, McGraw-Hill, London.

Vagelopoulos, C., and Egolfopoulos, F. 1998. Direct experimental determination of laminar flame speeds. *Symp. (Int.) Combust.*, **27**, 513–519.

Worth, N., and Dawson, J. 2013a. Modal dynamics of self-excited azimuthal instabilities in an annular combustion chamber. *Combust. Flame*, **160**, 2476–2489.

Worth, N., and Dawson, J. 2013b. Self-excited circumferential instabilities in a model annular gas turbine combustor: Global flame dynamics. *Proc. Combust. Inst.*, **34**, 3127–3134.